1 June 2001

ELSEVIER

Optics Communications 192 (2001) 399–405

OPTICS COMMUNICATIONS

www.elsevier.com/locate/optcom

Attractors and auto-oscillations for feedback controlled photorefractive beam coupling

E.V. Podivilov [a], B.I. Sturman [a], S.G. Odoulov [b], S.L. Pavlyuk [b], K.V. Shcherbin [b], V.Ya. Gayvoronsky [c], K.H. Ringhofer [c], V.P. Kamenov [c,*]

[a] *Institute of Automation and Electrometry, Koptyug Ave. 1, 630090 Novosibirsk, Russia*
[b] *Institute of Physics, National Academy of Sciences, 03650 Kiev, Ukraine*
[c] *Department of Physics, Osnabrück University, D-49069 Osnabrück, Germany*

Received 11 December 2000; received in revised form 3 April 2001; accepted 3 April 2001

Abstract

We investigate the physics of a novel nonlinear system, feedback controlled photorefractive beam coupling. Inertia of the electronic feedback is found to be an element crucial for permanent operation of this system. Theoretically and experimentally we have found a wealth of periodic and quasi-periodic regimes for observable characteristics of the feedback controlled wave coupling. A good qualitative agreement between theory and experiment is obtained for $LiNbO_3$ crystals. © 2001 Elsevier Science B.V. All rights reserved.

PACS: 42.40; 42.65

Keywords: Feedback; Attractors; Photorefractive; Diffractivity; Grating; Stabilization

1. Introduction

Several exciting research areas such as spatial solitons [1–3], pattern formation [4–6], subharmonic generation [7–9], and feedback controlled beam coupling [10–13], have arisen in recent years in the field of photorefractive nonlinear phenomena. The last topic stands separately in this list in the sense that it has, to our knowledge, no direct analogues among the nonlinear wave phenomena. This is greatly due to the big inertia of the photorefractive nonlinearity which allows to send a controlling electronic signal from output to input with no big delay and to modify strongly the characteristics of wave coupling.

In spite of the fact that feedback controlled dynamic systems are under extensive study for at least 10 years [14,15], the history of the feedback controlled coupling of optical waves is rather short. Initially, it was found empirically [10–12] that a certain electronic feedback loop between the output and input signal beam, controlling the input phase φ_s (see Fig. 1) produces dramatical changes in the dynamics of two-wave coupling as well as in the diffractive properties of the spatial index grating. It has been shown that application of the feedback to nonlinear media with the local

* Corresponding author. Fax: +49-541-969-2351.
E-mail address: vlado@physik.uni-osnabrueck.de (V.P. Kamenov).

0030-4018/01/$ - see front matter © 2001 Elsevier Science B.V. All rights reserved.
PII: S0030-4018(01)01210-X

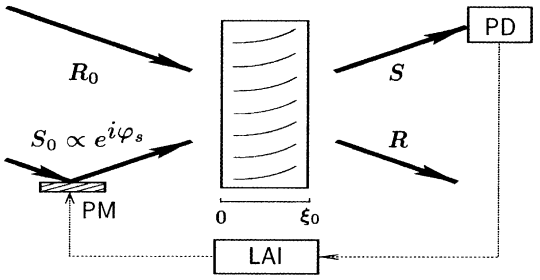

Fig. 1. Schematic of experiment; PD is a photodiode, LAI a lock-in amplifier and integrator, PM a piezo-mirror.

response (unshifted refractive index grating) leads, apart from stabilization of the interference pattern [16], to 100% diffraction efficiency of the recorded grating, to an efficient steady-state intensity coupling of the recording beams, and to suppression of light-induced scattering. The same technique can produce a controllable phase shift between zero order diffracted wave and first order diffracted wave propagating in the same direction [17].

The first formulation of the feedback problem in the terms of equations for beam coupling and boundary conditions was proposed in 1997 [13]. Despite its apparent simplicity, the problem proved to be resistant to the application of analytical tools. This is caused by the peculiarity of the situation, where the temporal development of a distributed nonlinear system is governed by strongly nonlinear feedback conditions coupling wave amplitudes and phases on opposite crystal faces.

Numerical simulations of the found equations have shown [13] that within a short time the system evolves to a state where the grating is fully diffractive or transparent and the formulated feedback conditions (that we call the ideal feedback conditions) fail. Thus the formulated mathematical model remains correct only within a restricted time interval. It is not capable of describing the whole evolution of the nonlinear system that operates permanently in experiment.

We have overcome the inherent defect of the previous studies taking into account inertia of the feedback loop. This has allowed to gain insight into the exciting physics of a novel nonlinear system. The purpose of this paper is to present the essence of the results obtained for the first time. Instead of steady states familiar for photorefractive schemes, our theoretical and experimental studies have revealed a wealth of periodic and quasi-periodic regimes for the feedback controlled two-wave coupling as well as a variety of transitions between them. The found regimes include doubling and tripling of the period, that correspond to different attractors in the configuration space, as well as various critical phenomena.

2. Basic relations

Let the reference (R) and signal (S) beams be incident onto the crystal (see Fig. 1). These beams build a dynamic refractive index grating and diffract from this grating. The set of equations for two-beam coupling we present in the general dimensionless form [13],

$$\partial_\xi R = \mathrm{i}ES, \tag{1}$$

$$\partial_\xi S = \mathrm{i}E^*R, \tag{2}$$

$$(\partial_\tau + 1)E = \mathrm{e}^{\mathrm{i}\theta}RS^*. \tag{3}$$

Here ξ and τ are coordinate and time, R and S the complex amplitudes of the reference and signal beams, E is the grating amplitude, and θ the characteristic phase. The coordinate ξ varies from 0 to ξ_0.

The set (1)–(3) is valid for many particular models of the photorefractive nonlinearity. Specification of the dimensionless parameters for the simplest models can be found in Ref. [18]. Eqs. (1) and (2) describe mutual diffraction of R- and S-beams from the grating. The total light intensity remains constant during propagation, $|R|^2 + |S|^2 = 1$. Eq. (3) describes buildup of the grating by the light interference pattern. The phase θ characterizes the type of the photorefractive response and ranges from 0 to 2π. For the local photorefractive response one can set $\theta = 0$.

Most experiments on the subject have been performed with $LiNbO_3$ crystals where the index grating buildup is due to the photovoltaic charge transport and the linear electro-optic effect [18,19]. We have here $|\theta| \ll 1$, $\xi = gx$, and $\tau \simeq t/t_\mathrm{d}$, where x and t are the real coordinate and time, t_d is the

dielectric relaxation time, $g \simeq \pi n^3 r E_{pv}/\lambda$, n the refractive index, λ the wavelength, r the relevant electro-optic coefficient, and E_{pv} the photovoltaic field. Typically, t_d ranges from 10^1 to 10^3 s. If the light polarization is extraordinary, we have a numerical estimate, $g\ (\mathrm{cm}^{-1}) \simeq 2E_{pv}$ (kV/cm), for $\lambda \simeq 530$ nm. The photovoltaic field in $LiNbO_3$ ranges from a few tens to $\simeq$100 of kV/cm. Hence the thickness $x_0 \simeq 1$ mm corresponds to $\xi_0 = g x_0 \gg 1$.

To formulate the feedback equations, we represent R and S as sums of the diffracted and transmitted components,

$$R = R_0\mathcal{R}_r + S_0\mathcal{R}_s, \qquad S = R_0\mathcal{S}_r + S_0\mathcal{S}_s. \tag{4}$$

The fundamental amplitudes $\mathcal{R}_r(\xi)$, $\mathcal{S}_r(\xi)$ satisfy Eqs. (1) and (2) with boundary conditions $\mathcal{R}_r(0) = 1$, $\mathcal{S}_r(0) = 0$. They describe testing of the spatial grating by a single beam of unit amplitude incident in R-direction (see Fig. 1). Analogously, $\mathcal{R}_s(\xi)$, $\mathcal{S}_s(\xi)$ is the solution of Eqs. (1) and (2) with boundary conditions $\mathcal{R}_s(0) = 0$, $\mathcal{S}_s(0) = 1$, which correspond to testing of the grating by a unit S-beam. One can check further that $\mathcal{S}_s = \mathcal{R}_r^*$ and $\mathcal{R}_s = -\mathcal{S}_r^*$. The quantity $\eta = |\mathcal{S}_r|^2 \equiv 1 - |\mathcal{S}_s|^2$ is the diffraction efficiency of the grating. The dependences of η, $\mathcal{S}_s$, and $\mathcal{S}_r$ on τ are governed by Eq. (3).

Next, we introduce the phase difference Φ_s between the diffracted and transmitted components of the S-beam at the output. According to Eq. (4)

$$\Phi_s = \varphi_r + \arg[\mathcal{S}_r(\xi_0)] - \varphi_s - \arg[\mathcal{S}_s(\xi_0)], \tag{5}$$

where $\varphi_r = \arg(R_0)$ and $\varphi_s = \arg(S_0)$ are the input phases of the R- and S-beams. Then the ideal feedback conditions read $\Phi_s = \pm\pi/2$. For nonzero $\mathcal{S}_s(\xi_0)$ and $\mathcal{S}_r(\xi_0)$, i.e. for $\eta(1-\eta) \neq 0$, we can fulfill them by adjusting φ_s and keeping $\varphi_r =$ const. If $\mathcal{S}_s(\xi_0)$ or $\mathcal{S}_r(\xi_0)$ is zero, the conditions $\Phi_s = \pm\pi/2$ make no sense. This circumstance is fatal for the ideal feedbacks that lead inevitably to states with $\eta(1-\eta) = 0$ [13].

In experiment, the phase adjustment is accomplished by a modulation technique. An auxiliary (small and fast) oscillating component, $\delta\varphi_s = \psi_d \sin\omega\tau$, is introduced into φ_s. It does not affect the grating buildup and serves for initiation of the feedback loop. The auxiliary phase modulation results in replacement of S_0 by $S_0 \exp(i\psi_d \sin\omega\tau)$ in Eq. (4) so that the output intensity $|S(\xi_0,\tau)|^2$ acquires HF components oscillating as $\sin\omega\tau$ and $\cos 2\omega\tau$. The amplitude of the second harmonic, which serves as an error signal in an electronic feedback loop, is $I_{2\omega} = 0.5|R_0S_0|(\eta(1-\eta))^{1/2}\psi_d^2\cos\Phi_s$. The error signal produces a mirror displacement $\propto \varphi_s$. The essence of the feedback controlled motion of the mirror is that its velocity is proportional to $I_{2\omega}$. This leads to the inertial feedback equation for the time derivative $\dot{\varphi}_s$,

$$\dot{\varphi}_s = \mp\frac{1}{\tau_f}|R_0S_0|\sqrt{\eta(1-\eta)}\cos\Phi_s, \tag{6}$$

where τ_f is the response time of the feedback loop. This time incorporates the amplification and integration of the error signal. It has to be very small, $\tau_f \ll 1$, to make the feedback operative. Inertia becomes important when $\eta(1-\eta)$ approaches zero. The phase φ_s loses here the ability to follow the feedback signal and the phase Φ_s deflects strongly from its ideal value. As for the initial stage, where $\eta(1-\eta)$ is far from zero, the difference between the inertial and ideal feedbacks is very small.

3. Numerical simulations

As our simulations show, the inertial feedback operates permanently and exhibits a wealth of different regimes. Below we present the most prominent features of the nonlinear behaviour for different values of the input beam ratio $\beta = |S_0|^2/|R_0|^2$ and the value $\theta = 6.6\times10^{-2}$ representative for $LiNbO_3$.

Fig. 2 shows the evolution of φ_s, η, and $\cos\Phi_s$ for $\tau_f = 10^{-3}$, $\xi_0 = 6.6$, and $\beta = 4$. After an initial stage, $0 < \tau \lesssim 1$, the input phase φ_s shows a regular but not periodic behaviour. It is characterized by almost periodic upward steps of $\simeq$340°. The time distance between them is $\simeq$0.35. The steps produce a considerable positive average slope of $\varphi_s(\tau)$, i.e., a frequency detuning $\Omega_s \gg 1$ for the input S-beam. The step-like phase growth is accompanied by apparently periodic (with a fine

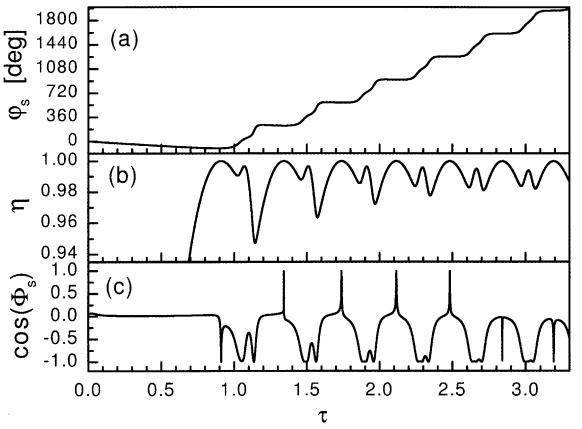

Fig. 2. Dependences $\varphi_s(\tau)$, $\eta(\tau)$, and $\Phi_s(\tau)$ for $\beta = 4$.

structure) oscillations of η in the vicinity of 1. The oscillation period ($\simeq$0.35) equals the distance between the phase steps. The phase Φ_s remains near $\pi/2$ only during the initial stage; further development is characterized by strong oscillations of $\cos\Phi_s$. Increase of τ makes the steps of φ_s and the oscillations of η and $\cos\Phi_s$ strictly periodic.

The closed line in Fig. 3a exhibits the relevant trajectory $\mathcal{S}_s(\xi_0,\tau)$ in the complex plane for $6 \leqslant \tau \leqslant 8$. About seven revolutions occur during this time. Thus the point $\Re\mathcal{S}_s(\xi_0,\tau), \Im\mathcal{S}_s(\xi_0,\tau)$ moves along a limit cycle (an attractor). This motion is periodic in time, its period, $T \simeq 0.35$, is the same as that of $\eta(\tau)$ and $\cos\Phi_s(\tau)$. The motion of $\mathcal{S}_r(\xi_0,\tau)$, that corresponds to the attractor, is a motion with small constant angular velocity Ω_r along the unit circle $|\mathcal{S}_r| \simeq 1$ superimposed by fast T-periodic oscillations.

How to combine the periodic behaviour of $\mathcal{S}_s$ and η with nonperiodic behaviour of $\mathcal{S}_r$ and φ_s taking into account that all these variables enter Eq. (6)? To clarify this, we set $\varphi_s = \varphi_s^p + \Omega_s\tau$, $\arg[\mathcal{S}_r] = \arg[\mathcal{S}_r]^p - \Omega_r\tau$, where φ_s^p and $\arg[\mathcal{S}_r]^p$ are T-periodic components. Then the only possibility to satisfy Eq. (6) is to demand that

$$(\Omega_s + \Omega_r)T = 2\pi N, \quad \text{with } N = 0, \pm1, \pm2 \ldots \qquad (7)$$

The number N depends on the attractor topology and may be called topological charge. For Fig. 3a we have $N = 1$.

A surprising feature of the described behaviour is the relatively long oscillation period, $T \simeq 0.35 \gg \tau_f$. To investigate the dependence $T(\tau_f)$, we have performed a numerical experiment: Starting from $\tau = 12$ (when the periodic state for $\beta = 4$ is achieved) we decreased τ_f from 10^{-3} to 4×10^{-5} during $\tau = 120$, causing adiabatic changes of the periodic solution. During this procedure, the attractor preserved a bagel-like form whereas the period T and the average $\langle 1 - \eta\rangle_T$ decreased. The following scaling relations were found: $T \simeq 7(\tau_f/|R_0S_0|)^{1/2}$, $\langle 1 - \eta\rangle_T \simeq 3.3\tau_f/|S_0R_0|$. They show that the fast oscillations of φ_s and Φ_s remain strong even when $\tau_f \to 0$.

Next we set $\beta = 6$. Fig. 3b shows the corresponding attractor. It consists of two loops and has a smaller transverse size. The zero point is at the central part of the orbit. An adiabatic decrease of τ_f results in a gradual decrease of the attractor size without remarkable changes of the form. The topological charge is 0 here. Fig. 4a gives the dependence $\varphi_s(\tau)$ for the periodic state. The average

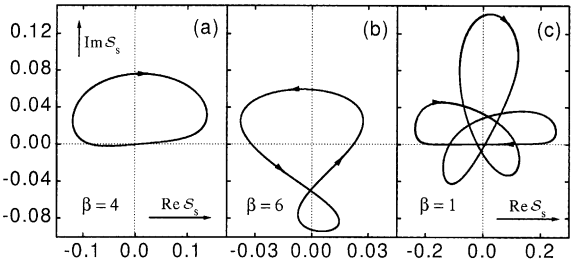

Fig. 3. Attractors for $\xi_0 = 6.6$, $\tau_f = 10^{-3}$, and three values of β.

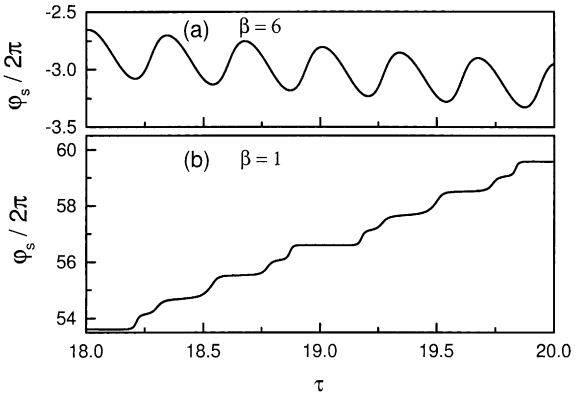

Fig. 4. Dependence $\varphi_s(\tau)$ for (a) $\beta = 6$ and (b) $\beta = 1$.

slope is negative, $\Omega_s \simeq -0.924$, and much smaller than for $\beta = 4$, the fine structure is not step-like but oscillatory, and $T \simeq 0.33$. Note that the values of $\varphi_s(\tau)$ in Fig. 4 correspond to $\varphi_s(0) = 0$. The choice of the initial phase does not influence indeed the physical characteristics of the system.

Now we consider the case $\beta = 1$. The temporal development ends up here by attraction to a new limit cycle, Fig. 3c. The full period T corresponds here to three revolutions around zero. This leads to a period tripling for $\varphi_s(\tau)$ and $\eta(\tau)$. The attractor size is larger than earlier, which gives larger oscillations of η in the vicinity of 1. The topological charge $N = 3$. Fig. 4b shows the dependence $\varphi_s(\tau)$. Here $T \simeq 0.97$, which is $\simeq$3 times larger than earlier, and $\Omega_s \simeq 19.3$. The phase dependence exhibits three substeps within a period.

Further variations of β give no qualitatively new attractors for $\xi_0 = 6.6$. The transitions between the periodic solutions with changing β are, however, far from trivial. Fig. 5 shows what happens with the bagel-like attractor when we slowly increase β from 6.6 to 8. Initially, gradual changes of the bagel occur. With β approaching $\simeq$6.8 these changes accelerate and within interval $6.8 \lesssim \beta \lesssim 7.3$ (which took $\tau \approx 15$) the trajectory becomes apparently irregular. Then, for $\beta \simeq 7.4$ a new attractor with $N = 0$ is formed. The above transition is very pronounced for the time dependence $\varphi_s(\tau)$. The change of the average slope Ω_s is very sharp despite of an irregular behaviour of the corresponding trajectories.

The transition between the three- and one-loop attractors (see Fig. 3c and a) occurs differently.

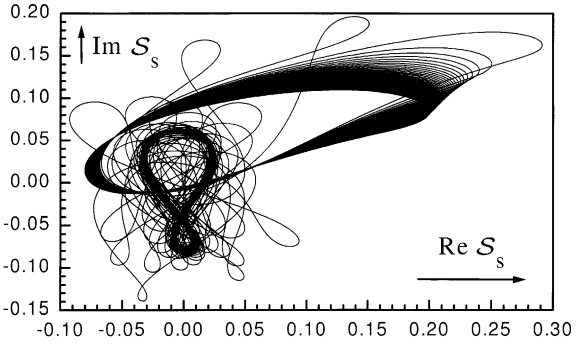

Fig. 5. Trajectory $\mathcal{S}_s(\xi_0, \tau)$ for $\beta(\tau)$ increasing from 6.6 to 8.

With β increasing from 1 to 2 a gradual convergence of different loops takes place. It is not accompanied by the change of the average slope Ω_s but means that the topological charge $N = 3$ transforms into $N = 1$.

In the region of large beam ratios, $\beta \gtrsim 20$, when we are near the threshold of auto-oscillations, a slowing down of the transient processes, typical of critical phenomena [20], takes place. For $\beta > 22$, auto-oscillations are absent and $1 - \eta$ is far from 1. Increasing ξ_0 expands the region of β yielding oscillatory regimes. An adiabatic increase of ξ_0 from 6.6 to 15 has not shown any transition to chaos typical of many feedback controlled dynamic systems [14,15].

4. Experiment

In our feedback experiments we used a 0.35 μm thick $LiNbO_3$:Fe crystal. A cw single-frequency frequency-doubled YAG:Nd^{3+} laser is used as the light source. Two extraordinary waves impinge upon the sample in the plane containing the crystal c-axis. The total light intensity at the sample input face is $\simeq$45 mW/cm^2 in all experiments. A free-space angle between the recording beams $2\theta_p \simeq 12°$ is chosen to ensure a relatively weak diffusion field ($E_D \simeq 650$ V/cm for grating spacing $\Lambda \simeq 2.5$ μm at 532 nm, while the photovoltaic field is estimated as $E_{pv} \approx 100$ kV/cm). The recorded volume grating is thick according to the Klein criterium [21]. Correspondingly, the higher diffraction orders were negligibly small. For the extraordinary polarized beams the dimensionless thickness $\xi_0 \approx 8$.

The design of our setup is similar to that described in Ref. [10–16]. The feedback is implemented with the help of a lock-in amplifier, summator/integrator, and piezodrive with maximum displacement of 15 μm. The piezo-mounted mirror placed in one of two interferometer lags introduces a small amplitude (0.1 rad) fast (500π rad/s) sinusoidal phase modulation of the signal wave. This frequency is large enough to use the self-stabilization technique with $LiNbO_3$ at the specified intensity. The signal beam intensity is measured by a photodetector connected to the

input of the lock-in amplifier. This lock-in amplifier is tuned to measure the second harmonic term of the transmitted signal beam intensity $I_{2\omega}$. Any nonzero error signal from the lock-in amplifier is accumulated in the analogue integrator feeding the piezoelectric-supported mirror. This results in a mirror displacement which changes the phase of the input signal beam until the error signal turns to zero. In such a way, $I_{2\omega}$ is minimized in the negative feedback loop to ensure the self-stabilized recording. The output of the integrator is automatically reset to zero when driving voltage of the piezoelectric-supported mirror reaches a certain limiting value defined by the piezo-driver specifications.

To verify the fact that the described electronic feedback meets the inertial condition (6), we have measured the transmission factor of the integrator $K_{\omega'}$ (output voltage/input voltage) as a function of the frequency ω' of an input harmonic signal. It was found that $K_{\omega'} \propto (\omega')^{-1}$ within a wide frequency range $\omega' \leqslant 10^2\ \mathrm{s}^{-1} \approx 10^4 t_\mathrm{d}^{-1}$, where $t_\mathrm{d} \approx 180$ s is the crystal response time at the specified intensity. Therefore the Fourier component of the mirror displacement $x_{\omega'} \propto (\omega')^{-1}$ and the Fourier component of the mirror velocity, $-\mathrm{i}\omega' x_{\omega'}$, does not depend on the signal frequency. This proves the validity of the linear relation (6) between $\dot{\varphi}$ and the error signal under the condition that the characteristic time of the intensity changes exceeds 10^{-3} s. This condition is fulfilled in experiment with a great safety margin. The value of the dimensionless response time of our feedback loop can be estimated as $\tau_\mathrm{f} \approx 10^{-4}$.

Now we turn to the description of the experimental results. For sufficiently large and small beam ratios, $\beta \gtrsim 50$ and $\beta \lesssim 0.03$, we did not observe any auto-oscillations. The diffraction efficiency remained here noticeably $\leqslant 1$.

Within the interval $0.03 < \beta < 50$ we have observed a variety of well recognizable oscillatory regimes with permanently working feedback and diffraction efficiency very close to 1. We have detected all the regimes presented above. Fig. 6a shows a typical fragment of the feedback controlled dependence $\varphi_\mathrm{s}(t)$ for $\beta = 10$ in the real time scale. A large average slope and quasi-periodic phase steps are clearly seen in this plot. These elements are similar to those presented in Fig. 2a. The time distance between the subsequent steps $\simeq 0.2 t_\mathrm{d} \simeq 36$ s. Fig. 6b corresponds to $\beta = 6.6$. It shows a considerably smaller slope and clearly pronounced quasi-periodic phase oscillations. The period of the oscillations is estimated here as $\simeq 0.3 t_\mathrm{d}$. These features are similar to the presented in Fig. 4a. Fig. 6c shows a representative dependence $\varphi_\mathrm{s}(t)$ for $\beta = 1$, it corresponds to the period tripling, compare with Fig. 3a. The full period, $\approx 0.82 t_\mathrm{d}$, is approximately 3 times larger than it is in the previous case.

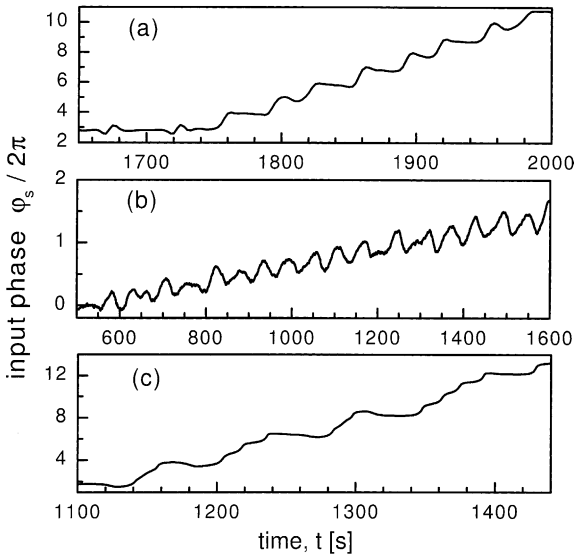

Fig. 6. Fragments of experimental dependences $\varphi_\mathrm{s}(t)$ for $\beta = 10$, 6.6, and 1.

The dependences of Fig. 6 illustrate experimental observation of the attractors. We cannot expect indeed an exact coincidence between the experiment and numerical simulations because of mechanical perturbations, air convection, and other factors affecting the experimental results and also because of some uncertainity in the values of the relevant material parameters. Nevertheless a good quantitative agreement is evident.

5. Summary

The results presented give an insight into the physics of a novel strongly nonlinear optical sys-

tem, the feedback controlled photorefractive beam coupling. We have formulated the governing equations for this nonlinear system that incorporate the essence of the feedback operation. For typical values of experimental parameters our numerical simulations have demonstrated a variety of qualitatively different periodic regimes (attractors) and nontrivial transitions between them. The theoretical results are in a good agreement with our experimental data for $LiNbO_3$:Fe crystals.

Acknowledgements

Financial support of INTAS and Deutsche Forschungsgemeinschaft is gratefully acknowledged.

References

[1] M. Segev, et al., Phys. Rev. Lett. 68 (1992) 923.
[2] M.F. Shih, M. Segev, G. Salamo, Phys. Rev. Lett. 78 (1997) 2551.
[3] W. Królikowski, et al., Phys. Rev. Lett. 80 (1998) 3240.
[4] T. Honda, Opt. Lett. 18 (1993) 598.
[5] A.V. Mamaev, M. Saffman, Phys. Rev. Lett. 80 (1998) 3499.
[6] S.G. Odoulov, et al., Phys. Rev. Lett. 83 (1999) 3637.
[7] B. Sturman, et al., J. Opt. Soc. Am. B 10 (1993) 1919.
[8] T.E. McClelland, et al., Phys. Rev. Lett. 73 (1994) 3082.
[9] H.C. Pedersen, P.M. Johansen, Phys. Rev. Lett. 77 (1996) 3106.
[10] A. Freschi, J. Frejlich, J. Opt. Soc. Am. B 11 (1994) 1837.
[11] P.M. Garcia, et al., Opt. Commun. 117 (1995) 35.
[12] P.M. Garcia, et al., Appl. Phys. B 63 (1996) 207.
[13] V.P. Kamenov, et al., Phys. Rev. A 56 (1997) R2541.
[14] E. Ott, C. Grebogi, J.A. Yorke, Phys. Rev. Lett. 64 (1990) 1196.
[15] R. Roy, T.W. Murphy, T.D. Maier, Z. Gills, E.R. Hunt, Phys. Rev. Lett. 68 (1992) 1259.
[16] A.A. Freschi, P.M. Garcia, I. Rasnik, J. Frejlich, K. Buse, Opt. Lett. 21 (1996) 152.
[17] A.A. Freschi, P.M. Garcia, J. Frejlich, Opt. Commun. 143 (1997) 257.
[18] L. Solymar, D.J. Webb, A. Grunnet-Jepsen, The Physics and Applications of Photorefractive Materials, Clarendon Press, Oxford, 1996.
[19] B.I. Sturman, V.M. Fridkin, The Photovoltaic and Photorefractive Effects in Noncentrosymmetric Materials, Gordon and Breach, Philadelphia, 1992.
[20] H. Haken, Advanced Synergetics, Springer, Berlin, 1983.
[21] W.R. Klein, Proc. IEEE 54 (1966) 803.